

FIRST RESULTS FROM THE *ISO-IRAS* FAINT GALAXY SURVEY¹

DEBORAH A. LEVINE,^{2,3} CAROL J. LONSDALE,² ROBERT L. HURT,² HARDING E. SMITH,^{4,2} GEORGE HELOU,²
 CHARLES BEICHMAN,² CATHERINE CESARSKY,⁵ DAVID ELBAZ,⁵ ULRICH KLAAS,³ RENE LAUREIJS,³
 DETRICH LEMKE,⁶ STEVEN LORD,² RICHARD MCMAHON,⁷ MEHRDAD MOSHIR,²
 GERRY NEUGEBAUER,⁸ B. T. SOIFER,⁸ DAVE VAN BUREN,²
 ANN WEHRLE,² AND RAY WOLSTENCROFT⁹

Received 1997 November 24; accepted 1998 April 3

ABSTRACT

We present the first results from the *ISO-IRAS* Faint Galaxy Survey (IIFGS), a program designed to obtain *ISO* observations of the most distant and luminous galaxies in the *IRAS* Faint Source Survey by filling short gaps in the *ISO* observing schedule with pairs of 12 μm ISOCAM and 90 μm ISOPHOT observations. As of 1997 October, over 500 sources have been observed, with an ISOCAM detection rate over 80%, covering over 1.25 deg² of sky to an 11.5 μm point-source completeness limit of approximately 1.0 mJy (corresponding to a $\sim 10\sigma$ detection sensitivity). Observations are presented for nine sources detected by ISOPHOT and ISOCAM early in the survey for which we have ground-based *G*- and *I*-band images and optical spectroscopy. The ground-based data confirm that the IIFGS strategy efficiently detects moderate-redshift ($z = 0.11\text{--}0.38$ for this small sample) strong emission line galaxies with $L_{60\mu\text{m}} \gtrsim 10^{11} L_{\odot}$; one of our sample has $L_{60\mu\text{m}} > 10^{12} L_{\odot}$ ($H_0 = 75 \text{ km s}^{-1} \text{ Mpc}^{-1}$, $\Omega = 1$). The infrared-optical spectral energy distributions are comparable to those of nearby luminous infrared galaxies, which span the range from pure starburst (e.g., Arp 220) to infrared QSO (Mrk 231). Two of the systems show signs of strong interaction, and four show active galactic nucleus (AGN)-like excitation; one of the AGNs, F15390+6038, which shows a high excitation Seyfert 2 spectrum, has an unusually warm far- to mid-infrared color and may be an obscured QSO. The IIFGS sample is one of the largest and deepest samples of infrared-luminous galaxies available, promising to be a rich sample for studying infrared-luminous galaxies up to $z \sim 1$ and for understanding the evolution of infrared galaxies and the star formation rate in the universe.

Subject headings: galaxies: active — galaxies: photometry — infrared: galaxies — surveys

1. INTRODUCTION

IRAS discovered thousands of luminous infrared-bright galaxies (LIGs), which emit most (over 90% in some cases) of their luminosity in the far infrared. These infrared-luminous galaxies dominate the space density of objects with $L > 10^{11} L_{\odot}$ (Soifer et al. 1987). Most of these objects are probably primarily powered by starbursts, but there is also evidence of active galactic nucleus (AGN) activity, especially at the higher luminosities (Sanders & Mirabel 1996). There has been speculation that protogalaxies may appear as high-redshift LIGs, but the two very high redshift systems, F10214+4724 and the Cloverleaf quasar, both appear to be lensed AGN systems (Eisenhardt et al. 1996; Barvainis et al. 1995).

The *IRAS* Bright Galaxy Sample (BGS) (Soifer et al. 1987), complete to 5.24 Jy at 60 μm , provides an excellent

sample of local infrared-luminous galaxies for studying the detailed emission mechanisms and starburst-AGN connections, but a determination of how these properties evolve with time, as well as searching for protogalaxy candidates, requires a large sample well distributed in redshift. The *IRAS* Faint Source Survey (FSS) (Moshir et al. 1992) contains over 750,000 sources to a 60 μm flux density limit as faint as 100 mJy in some regions of sky, which is over 50 times fainter than the limit of the BGS. The vast majority of these faint sources has not been followed up in any way. The *ISO* mission presents an ideal opportunity to obtain infrared spectral information for a subset of these objects, as well as much better positional information from ISOCAM than is available from the large *IRAS* 60 μm detectors.

The *ISO-IRAS* Faint Galaxy Survey (IIFGS) consists of 3776 of sources from the FSS,¹⁰ selected to be fainter than 300 mJy at 60 μm with galaxy-like infrared colors, to have galactic latitude greater than 30° (to avoid contamination by Galactic sources), and to have a high value of the infrared-optical flux density ratio, $\log(S_{60\mu\text{m}}/S_{\text{blue}}) \gtrsim 0.2$ for the northern hemisphere sample. The combination of faintness at 60 μm and the high value of $S_{60\mu\text{m}}/S_{\text{blue}}$ leads to a selection in favor of the most luminous and highest redshift candidates since there is a strong correlation between L_{FIR} and $L_{60\mu\text{m}}/L_{\text{blue}}$ for infrared-bright galaxies (Soifer et al. 1987). Blue magnitudes for each candidate source were

¹ *ISO* is an ESA project with instruments funded by ESA member states (especially the PI countries: France, Germany, the Netherlands, and the United Kingdom) and with the participation of ISAS and NASA.

² Infrared Processing and Analysis Center, Caltech/JPL, Pasadena, CA 91125.

³ *ISO* Science Operations Centre, Villafranca Apdo 50727, E-28080 Madrid, Spain.

⁴ Center for Astrophysics and Space Sciences, University of California, San Diego, CA 92093-0424.

⁵ Service d'Astrophysique, DSM, CEA-Saclay, F-91191 Gif-sur-Yvette Cedex, France.

⁶ Max-Planck-Institut für Astronomie, Königstuhl 17, D-69117 Heidelberg, Germany.


⁷ Institute for Astronomy, Madingley Road, Cambridge CB3 0HA, England.

⁸ California Institute of Technology, Pasadena, CA 91125.


⁹ Royal Observatory, Blackford Hill, Edinburgh EH9 3HJ, Scotland.

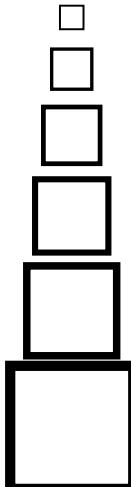
¹⁰ Sources were selected from the entire FSS, not just the Faint Source Catalog (FSC), to reach the faintest possible *IRAS* limits. Source reliability was assured by insisting on a good optical match to each source and a robust 60 mm detection on co-added scan tracks using IPAC's SCANPI processor.

Chart scale = 3.37 "/mm

COSCAT: \circ = gal, \bullet or \bullet = star
 GSC/TIC: \square = gal, \times = star
 FSDB (in center): 

COSCAT scale: Image size & shape
 GSC/TIC magnitude scale:

 9 11 12 13 14 15

 9 11 12 13 14 15

[14] [15] [16] [16] [17] [17]

[] = statistically corrected non-stellar mag.s

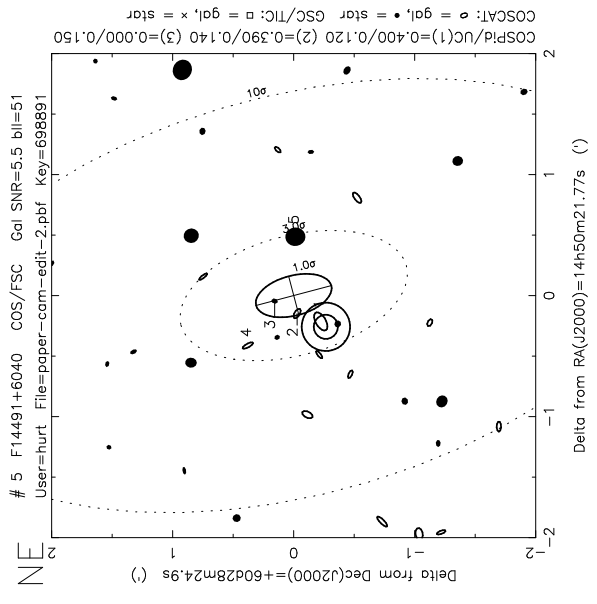
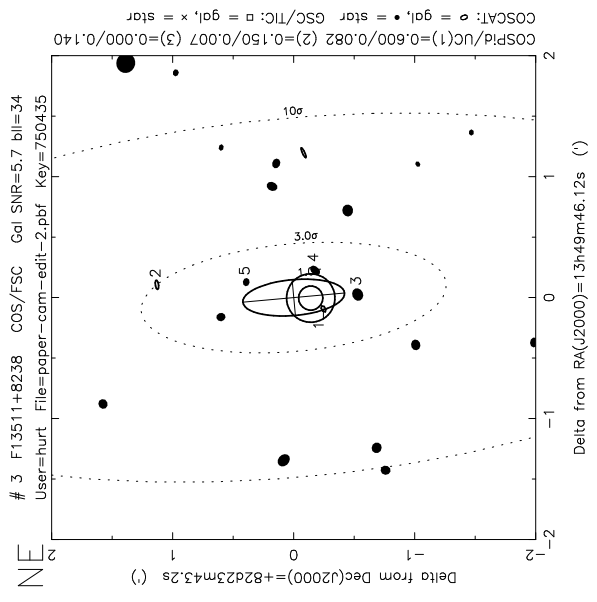
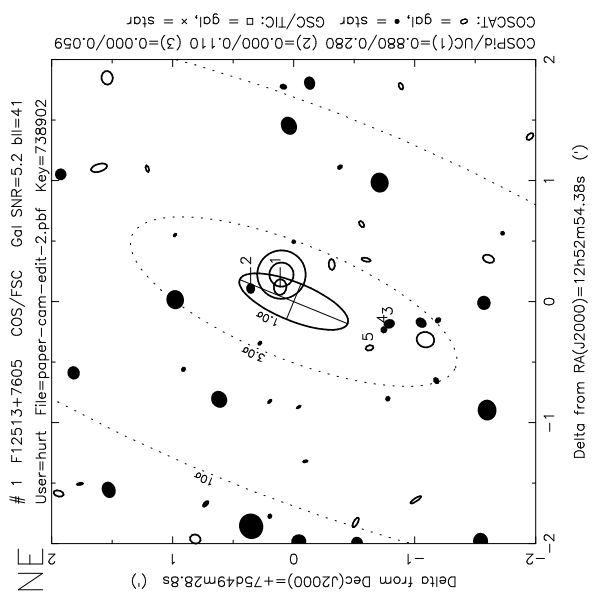
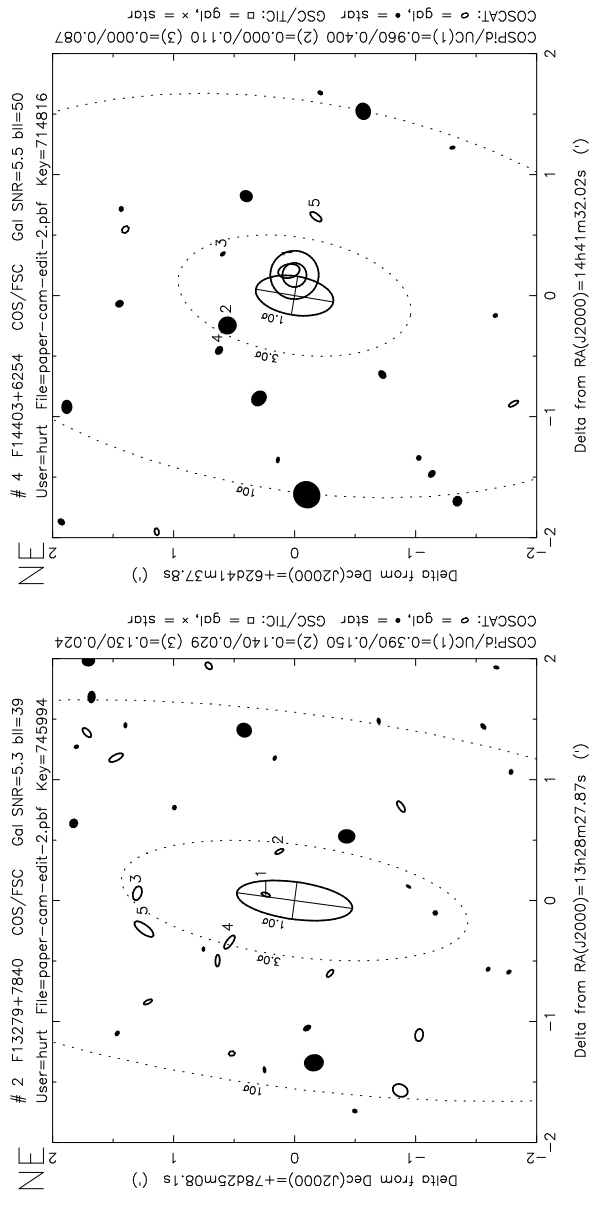


Fig. 1.—OPTID finding charts for the nine sources in our sample. Each chart is 4' on a side. Symbols for identification type (star vs. galaxy) are shown in the legend. Optical candidates are numbered in order of the identification probability assuming the APM classification and magnitude. The IRAS (1 σ) error ellipse is shown by the solid elliptical contour, and the CAM position is shown by the double circular contour, with radii 6" and 12". The position of the NVSS source in the field of F15390 + 6038 is indicated by the smaller double ellipse.

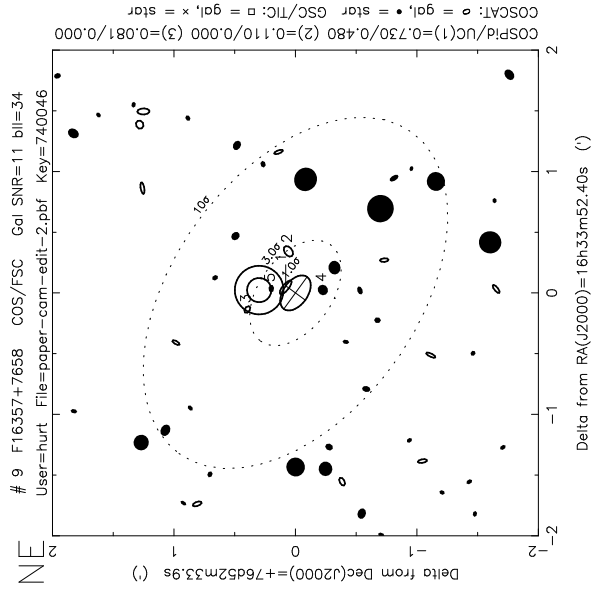
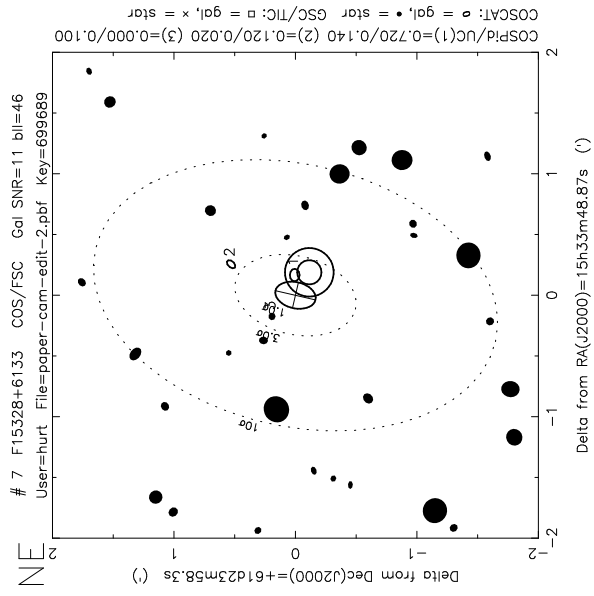
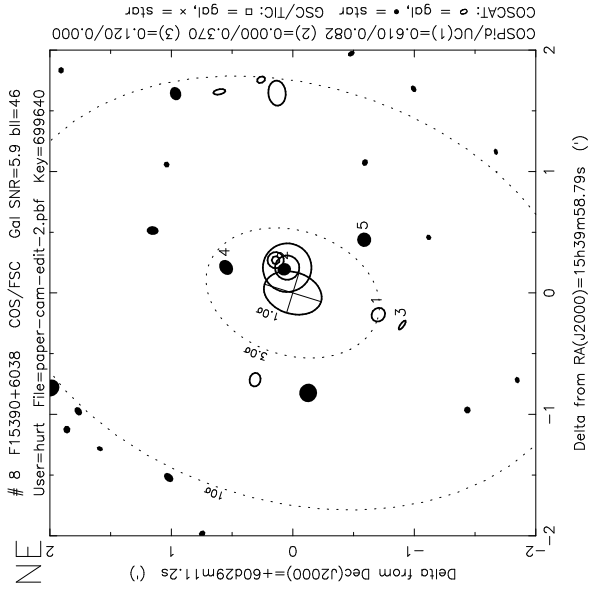
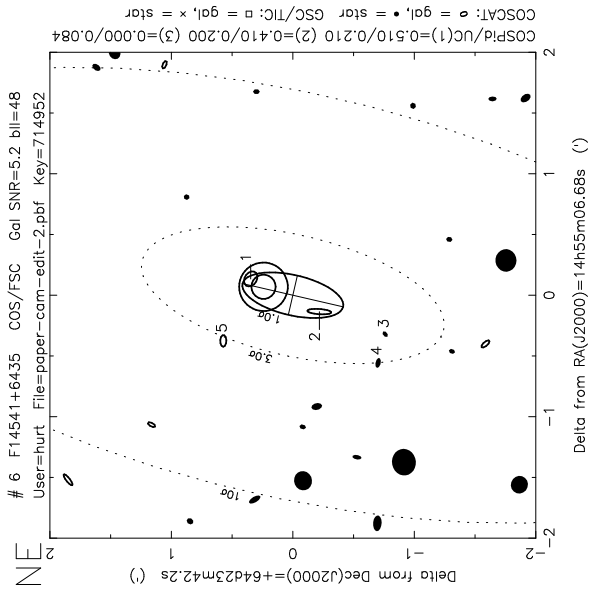


Fig. 1.—Continued

obtained from the IPAC's OPTID service (Lonsdale et al. 1997); 60 μm sources were selected if they have a blue counterpart fainter than about $17^{\text{m}}.5$ in the northern sky and 19^{m} in the southern sky (a lower magnitude limit was required in the north to obtain a comparable number of candidates in each hemisphere). Great care was taken to eliminate contamination by cirrus sources from the sample, but the effects of cirrus undoubtedly persist. The details of the source selection for the IIFGS are given elsewhere (Lonsdale et al. 1998b). OPTID finding charts for the nine sources reported here are shown in Figure 1.

The IIFGS sample galaxies are scheduled for observation by *ISO* on a "filler" basis; IIFGS sources are selected to fill gaps in the *ISO* observing schedule once higher priority targets have been scheduled. Thus the IIFGS serves to enhance the total observing efficiency of the mission. Of the 3776 candidate IIFGS sources in the *ISO* observation database, over 500 have been observed as of 1997 October, and it is expected that over 600 will be observed before the end of the *ISO* mission, with a total solid angle coverage of nearly 1.5 deg^2 on the sky. IIFGS source selection for *ISO* observation should be independent of source characteristics other than position on the sky. The nine sources presented here were selected for ground-based follow-up by the early availability of an ISOPHOT detection. This represents a potential bias in this small sample toward brighter $90 \mu\text{m}$ sources, but other factors, most notably *ISO* orbital position, time since curing of the detector, and presence of cirrus contamination, play a strong role in PHT noise and detection rate. This possible bias will not be fully understood until our entire PHT data set has been characterized, but we believe that it is small. Furthermore, preliminary analysis of the redshifts, spectral characteristics, and luminosities of a larger unbiased subset (Smith et al. 1998a) suggests that these nine sources are representative of the IIFGS as a whole.

The IIFGS sample will represent one of the best and largest deep samples of infrared-luminous galaxies until the advent of the Wide Field Infrared Explorer (WIRE) (Hacking et al. 1996) and SIRTF, even though it is based on selection from the 14 yr old *IRAS* survey. *ISO* cannot easily probe significantly deeper in redshift than the *IRAS* FSS because the excellent sensitivity of ISOCAM is offset by the declining infrared spectral energy distribution from $60 \mu\text{m}$ (the most sensitive *IRAS* band for galaxies) to the shorter mid-infrared wavelengths of ISOCAM.

2. OBSERVATIONS

Presented here are data for nine of the IIFGS galaxies obtained with the *Infrared Space Observatory* (*ISO*) (Kessler et al. 1996) by using the camera ISOCAM (Cesarsky et al. 1996) at $12 \mu\text{m}$ and the photometer ISOPHOT (Lemke et al. 1996) at $90 \mu\text{m}$. Optical spectra and *G*- and *I*-band images were obtained at Lick Observatory.

2.1. ISOCAM Observations

The ISOCAM data presented in this paper consist of short "microscan" maps that have been optimized for maximum sensitivity, by using the LW array, which is a 32×32 pixel gallium doped silicon array. The LW10 (*IRAS* $12 \mu\text{m}$) filter, centered at a wavelength of $11.5 \mu\text{m}$ was employed because of its large bandwidth of $7 \mu\text{m}$, and

the plate scale of $6'' \text{ pixel}^{-1}$ maximizes the collecting area of each pixel. Each field was observed using a 2×2 microscan with 5 pixel ($30''$) offsets in the satellite coordinate system, producing a fully sampled field of view of 2.7×2.7 . An integration time of 2.1 s was used for each frame. A typical observation consisted of 15 stabilization frames (allowing the detector to respond to the sky background), seven frames at each raster position, and two frames between rasters during slews, for an effective on-source integration time of about 60 s.

The ISOCAM data were reduced using custom software in development at IPAC. The Standard Processed Data product of the On-Line Processing versions 4.1–5.3 were employed for the reduction process. While a more detailed discussion of this technique will be forthcoming (Hurt et al. 1998), the basic steps are outlined here. Cosmic-ray hits are first identified and flagged using the multiresolution median deglitcher, MR1D_DEGLITCH,¹¹ which looks for glitches on short temporal scales and works well with unstabilized data. The next critical step is to correct for the "transient" response of the ISOCAM detectors. The time required for the detectors to stabilize to the zodiacal backgrounds in these fields is comparable to the length of our observations. In order to construct appropriate flat fields and co-add the data, this nonlinear, background-transient response must be removed from the data. We found the most productive approach to be to treat the transient as a baseline to be subtracted. A cubic curve is fitted to the time response for each pixel, allowing a floating window to mask out the step in signal attributable to a real source. Since each fully sampled sky position was observed in four different pixels, we are able to adjust the floating window iteratively to encompass the correct time ranges for the pixels contributing to a source detection.

Standard image processing techniques are used to produce mosaic images. The library dark current is subtracted from the baseline background model and is used to calculate a flat-field response for each pixel. The frames are aligned and co-added, weighted by the quality of the transient fit. Pixels with glitches and slew frames are excluded. Sources are identified in both space and time domains by examining both the mosaic and time history of each pixel; the sources reported in this paper are all strong, unambiguous detections. Photometric errors are estimated from the transient curve-fitting statistics, the weighted data averages, and the observed rms variation in the background of the mosaic; all error estimates agree to better than 10%.

Systematic errors introduced by this reduction process were measured for each field by applying the same processing after synthetic sources with a range of known flux densities were introduced. Our quoted flux densities have been corrected for these measured errors (typically 5%–30% in magnitude), and our photometric uncertainties have been estimated directly from the spread in recovered flux densities of these synthetic sources.

Photometric measures for each identified source are computed from the sum of each contiguous pixel detected at the 3σ level or better. A factor of $3.192 \text{ analog-to-digital converter unit mJy}^{-1} \text{ s}^{-1} \text{ gain}^{-1}$ was used to convert from

¹¹ A component of the CAM Interactive Analysis package, a joint development by the ESA Astrophysics Division and the ISOCAM Consortium.

detector units to mJy,¹² and the flux densities were further scaled upward by an empirical factor of 1.7 to account for the fact that faint sources will not reach their final stabilized responses in such short integrations. The uncertainties in calibrating nonstabilized data lead us to estimate an overall systematic calibration uncertainty of about 30%, in addition to the statistical errors. Faint ISOCAM source calibration is an ongoing area of investigation, so these measures should be considered preliminary indicators of the true 12 μm flux density. Positions were derived from flux-weighted averages for each contributing pixel and should be accurate to about 10", an error that is dominated by the uncertainty introduced by jitter in the lens wheel position.

A sample CAM image of the source F14491+6040 is shown in Figure 2b, compared with the Digitized Sky Survey image (Fig. 2a) and our *G*- and *I*-band images (Figs. 2c and 2d). The obvious CAM source represents a 17 σ detection, with 84% of the flux density in the brightest pixel.

2.2. ISOPHOT Observations

The ISOPHOT observations consist of chopped measurements with the C100 detector using the PHT-22 astronomical observing template (AOT). The broadest and most sensitive filter, C-90 with $\lambda_c = 95 \mu\text{m}$ and width 51.4 μm , was used for our investigations. The C100 camera consists of a 3×3 array with pixels 43.5 arcsec². At 90 μm about 60% of the Airy disk of a centered source is contained inside the central pixel. For the initial measurements, including the nine sources we discuss here, a 32 s total on-source integration time was used. ISOPHOT uses integrating amplifiers with nondestructive readout (NDR). Typical integration times are 0.5 or 1 s per "ramp," with 15 and 31 NDRs, respectively. Four ramps are taken per chopper plateau. A rectangular chopper mode was employed with an off-on separation of 180".

By using the default processing settings in version 6.1 of the ISOPHOT Interactive Analysis system (PIA) (Gabriel et al. 1997),¹³ 197 observations have been reduced. In addition, the nine sources discussed here were reduced carefully by hand using a test version of PIA 7.0; these hand-reduced data used the ramp subdivision option (normally with eight readouts per subramp) to have a larger number of effective integrations and thus enable better deglitching. The parameters for deglitching on the signal level were made slightly more stringent, and some particularly disturbed data were discarded by hand. Corrections for nonlinearity, reset interval time, and chopper vignetting were applied. No drift handling, modeling, or automatic deletion of data points were used. Additional corrections for "drift-related" effects (i.e., changes in detector response as a function in time) are discussed below.

One difficulty with the analysis of chopped C100 measurements is that the detector responses are not fully stabilized during the chopper plateau time. Since signal transient corrections have not yet been well determined, an empirical transient correction method has been established by com-

parison of special calibration data sets with fully stabilized, staring measurements. These comparisons indicate that chopped C100 measurements suffer a differential signal loss of a factor of 3, nearly independent of chopper frequency and source-to-background contrast (ISOPHOT Instrument Dedicated Team 1998).

The detectors also experience an increase in responsivity during an orbit largely due to cumulative effects of the radiation environment; this effect can sometimes be as large as a factor of 3. The internal fine calibration source (FCS) is intended to measure the responsivity at the time of observation; however, in chopped measurements the detectors are chopped between two FCS settings and the accuracy of responsivities derived this way has not yet been characterized. Fortunately, the value of the responsivity can be rather well predicted from the average response variation over several hundred *ISO* routine phase orbits, taking into account the orbital phase of the observation. This so-called orbit-dependent default responsivity (ISOPHOT Instrument Dedicated Team 19XX) was applied to each individual measurement as a function of the spacecraft orbital position. The uncertainty in the responsivity determined in this manner is estimated to be approximately 30%, with the highest uncertainty applying to measurements made close to the end of the science window where larger responsivity variations occur because of space weather activity. The flux densities obtained using this method are on average about 10% higher than those obtained using the chopped FCS measurement.

Flux densities were determined from the signal in the ISOPHOT central pixel (pixel 5) and were corrected for the point-spread function by dividing by the intensity fraction of a centered point source falling on a single C100 pixel (0.61 at 90 μm ; ISOPHOT Observers Manual version 3.1 1994, p. 14). The flux densities were further corrected for signal loss due to the offset of the source from the pixel center using a simple Gaussian beam model; these corrections range from a factor of 1.06 to 1.54. The correction was based on the position derived from the ISOCAM detection. There were several reasons for using the central pixel and applying these corrections, rather than integrating the signal over the whole array. In most cases the two measures did not diverge greatly, and in those cases where they did, significant cirrus contamination was suspected. It was also not possible to generate a good flat field for the limited number of observations, again due to the presence of cirrus, and the central pixel is relatively immune to flat-field problems. In most of the cases, the source was near the center of the central pixel and the amount of flux falling on the edge pixels would have been difficult to detect.

For the nine sources we have derived sensitivity limits based on the statistical noise in the on-off difference (i.e., ignoring the uncertainty of the calibration and considering the significance of the detection). The median 5 σ sensitivity for the central pixel (pixel 5) is about 185 mJy, ranging from 79 to 476 mJy. The effective sensitivity varies strongly from observation to observation because of the following factors:

1. The curing history of the detector; the detector is most stable directly following curing, which occurs daily just before the science window opens and again when the communications sites are changed, roughly at the middle of the orbit.
2. The cosmic particle rate, which can have serious

¹² From the current CCGLWSPEC calibration file (version 0711, 1996 July) as posted on the ESTEC *ISO* Observer Support Web site: http://isowww.estec.esa.nl/science/cal_g/cam_section.html.

¹³ The ISOPHOT data presented in this paper were reduced using PIA, which is a joint development by the ESA Astrophysics Division and the ISOPHOT consortium.

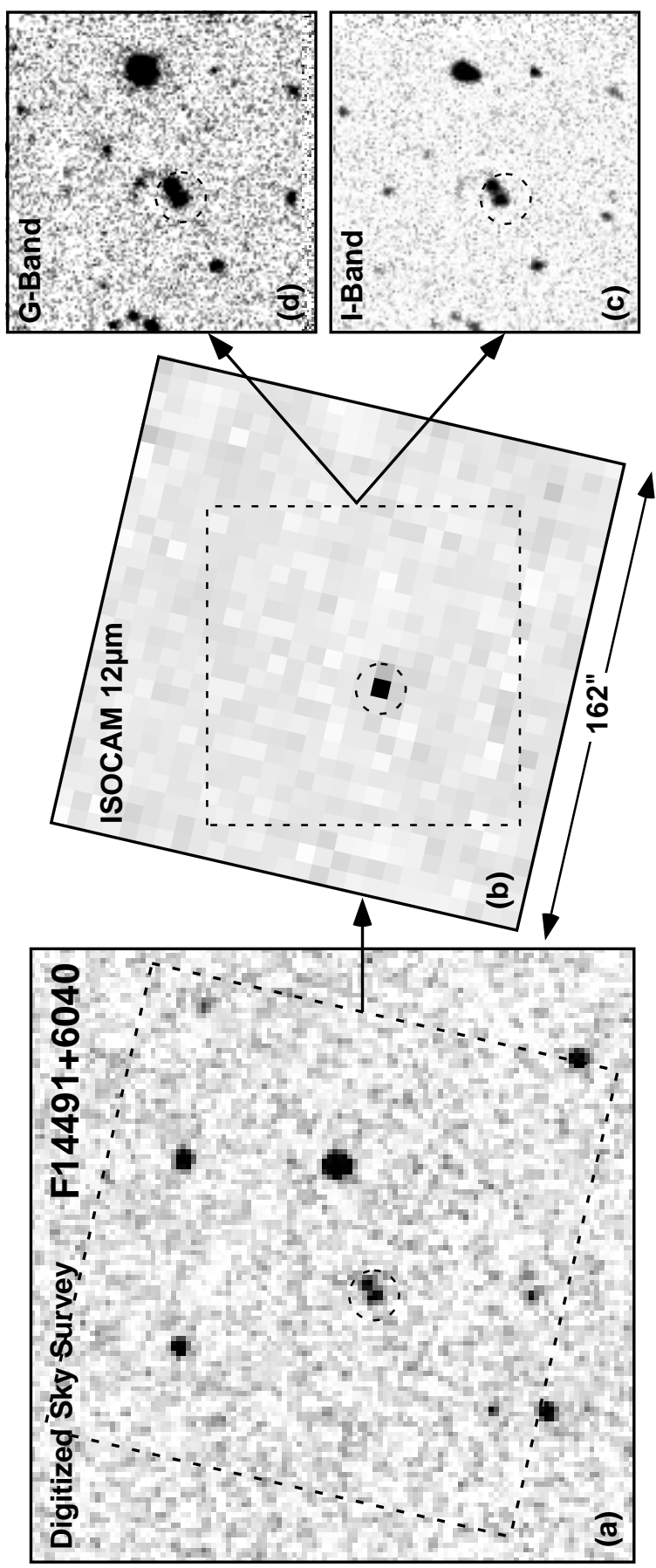


FIG. 2.—ISOCAM 11.5 μm and optical imaging of F14491 + 6040. (a) STScI Digitized Sky Survey image for this field. The region covered by the fully sampled ISOCAM image is indicated by the dashed box, and the location of the ISOCAM source is indicated by the dashed circle. (b) The ISOCAM image is rotated to match the Digitized Sky Survey image; the entire fully sampled image is shown, spanning 160" on a side. The field imaged at Lick Observatory is indicated by the dashed box. The Lick (c) G-band (44700) and (d) I-band (48275) images clearly show the double-nucleus counterpart to the ISOCAM detection as well as a probable tidal tail feature seen immediately to the north.

impact, especially toward the end of the science window when *ISO* is starting to enter the radiation belts.

3. The flux history of preceding measurements; serious transient effects can be introduced following observation of bright sources.

4. Strong glitches; severe particle hits introduce responsivity variations that last for an entire chopper plateau or longer, generating highly unreliable data for that interval.

The range of sensitivity for the observations reduced with the FCS calibration was similar, 16–421 mJy, again based on the data from the central pixel. These should remain representative of the detection limits of the survey data reduced using the empirical corrections for chopper signal loss and responsivity drift.

2.3. Source Identification Procedures

A three-way positional identification procedure was undertaken between the *IRAS* 60 μm position, the ISOCAM 12 μm position, and candidate optical matches using IPAC's OPTID service (Lonsdale et al. 1997), taking into account the intrinsic positional uncertainties at each wavelength. These were taken to be 15" at 12 μm and 1" for the optical data (1 σ), which is derived, for the northern sky, from POSS I plates digitized by the Automatic Plate Measuring Facility (APM) in Cambridge (Irwin et al. 1994).¹⁴ For *IRAS*, the major and minor 1 σ positional uncertainties listed in the FSS Database for each source were used. Full details of these identification procedures will be given in future papers (Hurt et al. 1998; Lonsdale et al. 1998c); a brief description is given here.

The combined *IRAS*-ISOCAM positional uncertainties (typically 17" \times 24", 1 σ) are large enough that the chance of false matches is significant. Therefore, we first did a two-way *IRAS*-ISOCAM positional match, employing a careful analysis of the probability distribution of the matches, following the reliability techniques developed by Lonsdale et al. (1997).¹⁵ We then performed a simple two-way ISOCAM-optical match procedure based on positional coincidence alone, since the optical positional uncertainties are only of order 1", to select the optical candidate match for observing at the telescope. The third leg of the

three-way match procedure was then completed by checking the probability that the selected optical object is the correct match to the *IRAS* source, using OPTID.

In six of the eight detected sources the optical match was indeed confirmed by OPTID as the best optical match to the *IRAS* source. The exceptions are F15390+6038 and F16357+7658, for which the best optical match to the CAM source was misclassified by the APM as a star rather than a galaxy. When optical source classifications are ignored, the CAM-optical match for F15390+6038 is then found to be the best optical match to the *IRAS* source. For F16357+7658, however, a galaxy at 16^h33^m51^s.6, +76°52'39" remains the best match to the *IRAS* source while a fainter galaxy at 16^h33^m51^s.8, +76°52'46" is the closest match to the ISOCAM detection. However, these two galaxies are apparently an interacting pair, separated by 7". Since this separation is small compared with the *IRAS*-ISOCAM combined positional uncertainty for this source (16" \times 18") it is likely that the 60 and 12 μm emission is associated with both galaxies of the pair, and integrated properties are therefore presented.

Details of the positional data are given in Table 1, which presents the *IRAS*-FSS position, the ISOCAM position, and the APM optical position, as well as the *ISO*-FSS, *ISO*-optical, and FSS-optical positional offsets. The FSS-optical offset is tabulated in units of the combined FSS-optical uncertainty, dominated, of course, by the uncertainty in the infrared position. Note that the ISOCAM-FSS separations are all smaller than the typical 1 σ uncertainty of 17" \times 24". There is evidence for a small systematic offset between the ISOCAM and the optical positions of 2"–3" in declination.

We searched the literature and on-line databases for positional matches of our sources with any other known source at any other wavelength. Only F15390+6038, the high excitation Seyfert 2 galaxy in our sample, has any match within an arcminute, in this case in the NRAO VLA Sky Survey (NVSS) radio database (Condon et al. 1997): NVSS J153956+602919, with 20 cm flux density, $S_{1.49\text{GHz}} = 3.6 \pm 0.4$ mJy, lies 6'7" from the ISOCAM position (see Fig. 1). The implied radio-infrared parameter, $q = 1.82$,¹⁶ for F15390+6038 is within the observed range for LIGs but is 0.5 dex below the mean value, $\langle q \rangle = 2.34$ (Condon, Anderson, & Helou 1991), providing further evidence that this is a

¹⁴ See also <http://www.ast.cam.ac.uk/lpinfo/apmcat/apmcat.html>.

¹⁵ A complicating factor in this procedure is that the background galaxy number counts at 12 mm must be known for this analysis, and these are as yet poorly defined. Thus, our identification procedures will refine with time as these counts become better measured.

¹⁶ The q -value is the dimensionless logarithmic far-infrared—60 mm plus 100 mm—to 1.49 GHz radio ratio (Condon et al. 1991).

TABLE 1
SELECTED *ISO-IRAS* FAINT GALAXIES: POSITIONAL OFFSET DATA

<i>IRAS</i> SOURCE	FSS POSITION		ISOCAM POSITION		OPTICAL POSITION		<i>ISO</i> -FSS		<i>ISO</i> -OPT		FSS-OPT σ^a
	α (J2000)	δ (J2000)	α (J2000)	δ (J2000)	α (J2000)	δ (J2000)	α (arcsec)	δ (arcsec)	α (arcsec)	δ (arcsec)	
F12513+7605.....	12 52 54.4	+75 49 29	12 52 50.7	+75 49 35	12 52 52.43	+75 49 35.5	13.7	−6.0	6.4	0.5	0.5
F13279+7840.....	13 28 27.9	+78 25 08	13 28 26.88	+78 25 22.4	0.5
F13511+8238.....	13 49 46.1	+82 23 43	13 49 46.3	+82 23 35	13 49 48.94	+82 23 28.4	−0.4	8.0	5.2	6.6	1.0
F14403+6254.....	14 41 32.0	+62 41 38	14 41 30.5	+62 41 38	14 41 30.25	+62 41 40.6	10.3	0.0	−1.7	2.6	1.2
F14491+6040.....	14 50 21.8	+60 28 25	14 50 23.9	+60 28 09	14 50 23.51	+60 28 11.5	−16.2	16.0	−3.6	2.5	1.7
F14541+6435.....	14 55 06.7	+64 23 42	14 55 06.0	+64 23 57	14 55 05.44	+64 24 03.0	4.5	−15.0	3.6	6.0	0.9
F15328+6133.....	15 33 48.9	+61 23 58	15 33 47.48	+61 23 58.7	1.5
F15390+6038.....	15 39 58.8	+60 29 11	15 39 57.1	+60 29 14	15 39 57.21	+60 29 15.4	12.6	3.0	0.8	1.4	1.1
F16357+7658.....	16 33 52.4	+76 52 34	16 33 52.0	+76 52 52	16 33 51.77	+76 52 45.8	6.4	−18.0	−0.8	−6.2	1.9

NOTE.—Units of right ascension are hours, minutes, and seconds, and units of declination are degrees, arcminutes, and arcseconds.

^a FSS-APM Optical positional offset in units of the combined FSS-Optical uncertainty.

TABLE 2
SELECTED ISO-IRAS FAINT GALAXIES: SPECTROSCOPIC RESULTS

Name	z	Detected Lines	[N II]/H α	[O III]/H β	Excitation
F12513 + 7605	0.1676	H α , N II	-0.26	...	H II/LINER
F13279 + 7840
F13511 + 8238	0.2718	H α , [N II], [O III]	-0.35	>0.5	H II:
F14403 + 6254	0.1117	H α , [N II], [S II]	-0.13	...	H II
F14491 + 6040a	0.2779	H α , [N II], [S II], H β , [O III]	-0.32	-0.18	H II
F14491 + 6040b	0.2783	H α , [N II], [S II], H β	-0.09	>0.5	AGN
F14541 + 6435	0.1995	H α , [N II], [S II]	-0.09	...	AGN/LINER
F15328 + 6133	0.3534	H α , [N II]	-0.40	...	H II
F15390 + 6038	0.3769	H α , [N II], [S II], H β , [O III]	-0.35	0.78	Seyfert 2; $\Delta v = 500 \text{ km s}^{-1}$ (FWHM)
F16357 + 7658	0.2714	H α , [N II], [S II], [O III]	0.00	>0.0	AGN/LINER

very active system. Although the fields of the other IIFGS sources are covered by the available NVSS survey database, none of the other sources is detected; this result is not surprising since IIFGS sources with normal q -values are at the limit of the NVSS.

2.4. Optical Imaging and Spectrophotometry

Ground-based imaging and spectrophotometry are being obtained for IIFGS galaxies at Lick and Palomar Observatories in order to obtain redshifts, morphology, and optical/near-infrared photometry. The sources presented here were observed in 1996 June with the Lick Observatory 3 m Shane Telescope using the Kast Imaging Spectrograph under photometric conditions with fair ($1''.5$) seeing. Spectra covering the wavelength region $\lambda\lambda 3500\text{--}10000$ at 5 \AA resolution were obtained for redshift determination, and imaging was obtained through “G” ($\lambda_c \approx 4700 \text{ \AA}$; $\Delta\lambda \approx 1215 \text{ \AA}$) and “I” ($\lambda_c \approx 8275 \text{ \AA}$; $\Delta\lambda \approx 1175 \text{ \AA}$) filters. The spectra were reduced with standard techniques using the IRAF reduction package. Virtually all of the galaxies showed strong emission lines characteristic of infrared galaxies. Redshifts are presented in Table 2, along with a list of the emission lines detected and a simple characterization of the excitation as AGN/Seyfert, LINER, or H II following the technique originated by Baldwin, Phillips, & Terlevich (1981, hereafter BPT). Although in principle both the [N II]/H α and [O III]/H β ratios are necessary, in some cases the [N II]/H α ratio is, by itself, sufficiently extreme to establish the excitation. The optical spectroscopic measures are comparable to nearby samples of LIGs, with values near the H II/LINER/AGN boundaries in the BPT excitation diagram (Smith, Lonsdale, & Lonsdale 1998). There is one clear Seyfert 2 galaxy, F15390 + 6038, which exhibits very high excitation and emission-line velocity widths, $\Delta v \approx 500 \text{ km s}^{-1}$. The median H α equivalent width, $W_{\lambda}^{\text{rest}} \approx 40 \text{ \AA}$, is comparable to that for nearby LIGs (Veilleux et al. 1995) and significantly larger than typical equivalent widths of nearby (nonstarburst) field galaxies (Kennicutt 1992).

Optical photometry was obtained from G ($\lambda 4700$) and I ($\lambda 8275$) band images obtained simultaneously through the Kast Spectrograph ($0''.78 \text{ pixel}^{-1}$, approximately $2'$ field of view). Typically five 100 s images were obtained in each filter, dithering the telescope by $5''\text{--}10''$ between images. Flat fields were obtained from median sky frames. The photometry was calibrated from filter transmission data kindly measured for us by Rem Stone at Lick Observatory, convolved with our spectrophotometry of the standard stars BD + 28 4211 and BD + 33 2642. Photometry was done using the IRAF APPHOT package with $7''$ apertures. Statistical error in the photometry is typically 1%–5%,

much smaller than our estimate of systematic error of approximately 10%–30% (1σ). As a sample of the data, the central section of our mosaic images of F14491 + 6040 is shown in Figure 2, and the spectrum of this interacting pair is shown in Figures 3a and 3b. Also shown in Figure 3c is the spectrum of F15390 + 6038, the highest excitation Seyfert 2 system in this sample.

3. RESULTS

The overall detection rates for the IIFGS sources are quite high: $\sim 80\%$ at $11.5 \mu\text{m}$ for 418 fields processed as of 1997 October and $\sim 50\%$ at $90 \mu\text{m}$ for 140 sources at the 5σ confidence level. These are fairly conservative estimates, which are expected to improve as knowledge of the ISO instruments and data processing techniques improve.

For the nine sources presented here, the ISOPHOT detection rate of 100% is not representative because sources were selected for spectroscopic observation based on detection by PHT. One source is not detected by CAM, and for this same source, F13279 + 7840, no redshift could be obtained from the spectrum. The remaining eight sources are all identified with strong emission-line galaxies. The fact that the emission lines are so strong is additional support for the validity of the optical identifications with the infrared sources, since the likelihood of false association of the infrared sources with such strong emission-line galaxies is very small.

Optical-to-far-infrared photometry for these nine sources is given in Table 3, along with derived colors and mid- to far-infrared luminosities ($H_0 = 75 \text{ km s}^{-1} \text{ Mpc}^{-1}$, $\Omega = 1$). The $60 \mu\text{m}$ flux densities are from the IRAS FSS; these sources represent some of the strongest $60 \mu\text{m}$ sources in our sample. Also presented are co-added IRAS scan data from IPAC’s SCANPI one-dimensional co-adder at both 60 and $100 \mu\text{m}$. Uncertainties listed for ISOCAM and ISOPHOT represent 1σ photometric errors; there is also an estimated uncertainty of order 30% for the absolute calibration of these observations.

There is a significant systematic difference between the IRAS SCANPI $100 \mu\text{m}$ flux densities and the PHT $90 \mu\text{m}$ data. We have carefully examined these fields, overplotting the ISOPHOT chop geometries on the appropriate IRAS Sky Survey Atlas plates. While the IIFGS fields were chosen to minimize cirrus contamination, cirrus is present in some of these IIFGS fields and is likely to affect the results for SCANPI and PHT in different ways, owing to the different observation modes: scanned versus chopped. In particular, chopping into cirrus will systematically reduce the PHT signal, while the SCANPI measures may be less sensitive to cirrus. We may ascribe the differences for most sources to a

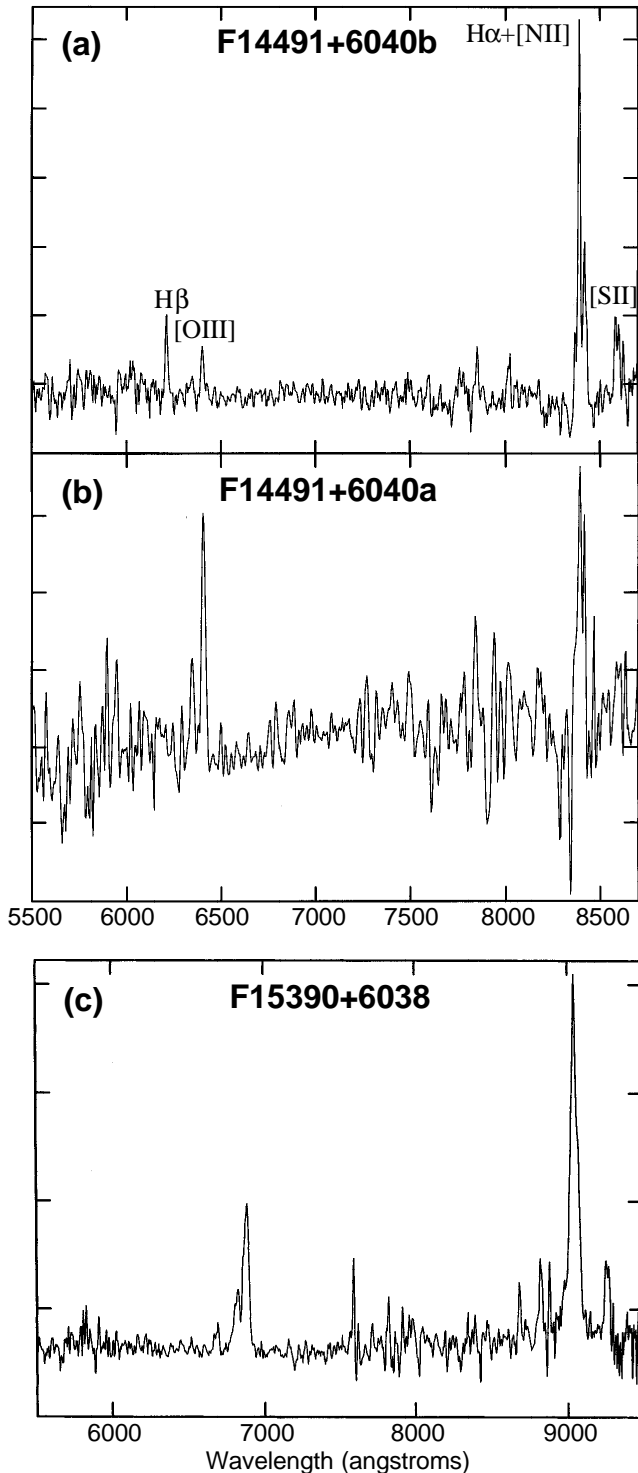


FIG. 3.—Lick Observatory red spectra of IIFGS LIGs. (a) F14491+6040a, $z = 0.2779$, is shown in Fig. 2 to be interacting; this member of the pair shows H π excitation. (b) F14491+6040b, $z = 0.2783$ (the redshift difference between F14491+6040a and F14491+6040b is not significant), shows AGN excitation. This spectrum has been lightly smoothed (3 pixel Gaussian). (c) F15390+6038, $z = 0.3769$, is the highest redshift galaxy in this sample of nine and the most clear case of Seyfert 2 excitation.

combination of two effects: (1) the remaining uncertainty in the PHT absolute calibration and (2) cirrus contamination. For two sources, F12513+7605 and F15328+6133, the above do not appear to be able to explain the apparent

disagreement; F15328+6133, with a discrepancy of a factor of 3, is a particularly messy field, but the simplest interpretation of the cirrus structure in this field would suggest that PHT may be chopping off a relatively broad cirrus plateau, possibly *overestimating* the flux density. It is the case that the sources with the largest *IRAS-ISO* discrepancies are in fields with the greatest cirrus contamination.

The spectral energy distributions for the nine sources are plotted in Figure 4. The spectra are shown with an arbitrary offset, and the mid-infrared spectral energy distributions (SEDs) generally grow flatter from the bottom to the top of the plot. In two cases, IPAC's *IRAS* scan co-addition processor, SCANPI, has provided us with additional *IRAS* data: $S_{12\ \mu\text{m}} = 0.05 \pm 0.03$ Jy for F15390+6038 and $S_{25\ \mu\text{m}} = 0.12 \pm 0.03$ Jy for F13511+8238, where the uncertainties include systematic effects due to cirrus noise as well as the photometric uncertainties; these data points are included in Figure 4. ISOCAM and ISOPHOT error bars include the 30% estimated uncertainty in absolute calibration. In each case the IIFGS galaxy SED is overplotted with the best match or matches from visual inspection of several characteristic nearby LIGs from Sanders et al. 1988. Three galaxies have SEDs that adequately fit most of the IIFGS data: Arp 220, an advanced merger and very dusty, compact nuclear starburst (e.g., Smith et al. 1998b; Sturm et al. 1996); UGC 5101, a high excitation Seyfert galaxy with an AGN radio core (Lonsdale, Lonsdale, & Smith 1995); and Mrk 231, a warm source with a strong Seyfert 1 active nucleus and a QSO-class bolometric luminosity, possibly a nascent quasar (Lonsdale et al. 1998a). An exception is F15390+6038, which is not well matched by any of our template LIGs; in this case all three SEDs are plotted for comparison. Three galaxies are reasonably well represented by the SED of UGC 5101, although two of these, F12513+7605 and F14403+6254 have a somewhat higher optical/mid-infrared flux-density ratio; in these cases the spectrum of Mrk 231 is also shown for comparison. F13511+8238 is well matched by Mrk 231. F15390+6038 has an unusual SED showing an exceptionally large mid- to far-IR flux-density ratio, but with a steep mid-IR to optical slope. One is tempted to use these SED relationships to draw inferences about the underlying energy sources for IIFGS galaxies, but comparison of the energy distributions with luminosity or optical spectral excitation does not show any clear relationship between AGN excitation or bolometric luminosity and IR-to-optical SED, similar to the case for nearby LIGs (Smith et al. 1998).

The observed redshifts agree well with the crudely predicted redshifts derived from the $L_{60\ \mu\text{m}}$ versus $L_{60\ \mu\text{m}}/L_{\text{blue}}$ relation for three sources. For the rest of the sources the predicted redshifts are too high; this is due to the fact that the *B*-band magnitudes measured from the archival Schmidt plate material by the APM measuring engine (as reported by OPTID) are systematically faint compared with the new *G*-band photometry by 0^m2-1^m5 , with the discrepancy increasing at fainter magnitudes. When the new photometry is used, all the objects lie on the same $L_{60\ \mu\text{m}}$ versus $L_{60\ \mu\text{m}}/L_{\text{blue}}$ relation as the BGS sample (Fig. 5a).

Two of the sources are identified with clearly interacting galaxy pairs: F14491+6040 and F16357+7658; and three others show weak signs of tidal distortion: F12513+7605, F14541+6435, and F15390+6038. Neither image profile fitting nor morphological classification has been attempted,

TABLE 3
SELECTED ISO-IRAS FAINT GALAXIES: PHOTOMETRIC PROPERTIES

IRAS Source	60 μm	11.5 μm	90 μm	60 μm	100 μm	B_{APM} (mag)	$\log \frac{S_{60}}{S_B}$	S_{4700} (G)	S_{8275} (I)	z_{pr}	z_{obs}	L_{60} ($\log L_{\odot}$)	L_{12} ($\log L_{\odot}$)	$\log \frac{S_{60}}{S_G}$
	FSS (mJy)	CAM (mJy)	PHT (mJy)	IRAS: SCANPI (mJy)	IRAS: SCANPI (mJy)									
F12513 + 7605.....	159 \pm 31	5.43 \pm 0.27	218 \pm 17	160 \pm 20	320 \pm 50	19.1	1.07	0.121 \pm 0.006	0.37 \pm 0.02	0.17	0.1676	11.12	10.29	1.02
F13279 + 7840.....	161 \pm 31	≤ 0.7 (3 σ)	202 \pm 63	170 \pm 20	≤ 400 (3 σ)	21.7	2.12	0.021 \pm 0.002	0.08 \pm 0.01	0.83	1.80
F13511 + 8238.....	180 \pm 32	15.31 \pm 0.43	168 \pm 19	210 \pm 20	440 \pm 150	21.6	2.12	0.084 \pm 0.004	0.17 \pm 0.01	0.80	0.2718	11.69	11.16	1.29
F14403 + 6254.....	163 \pm 30	4.59 \pm 0.27	241 \pm 50	220 \pm 30	350 \pm 100	19.8	1.36	0.150 \pm 0.008	0.61 \pm 0.03	0.26	0.1117	10.88	9.91	1.06
F14491 + 6040.....	135 \pm 25	2.86 \pm 0.18	151 \pm 24	140 \pm 20	≤ 400 (3 σ)	19.8	1.28	0.100 \pm 0.005	0.35 \pm 0.02	0.25	0.2780	11.54	10.43	1.04
F14541 + 6435.....	155 \pm 31	2.95 \pm 0.22	192 \pm 17	180 \pm 20	340 \pm 100	20.5	1.62	0.106 \pm 0.006	0.32 \pm 0.02	0.40	0.1995	11.33	10.24	1.12
F15328 + 6133.....	282 \pm 26	1.04 \pm 0.15	257 \pm 31	340 \pm 120	735 \pm 250	21.0	2.08	0.036 \pm 0.004	0.16 \pm 0.01	0.60	0.3534	12.15	...	1.87
F15390 + 6038.....	164 \pm 28	20.43 \pm 0.46	340 \pm 95	200 \pm 20	≤ 300 (3 σ)	20.4	1.64	0.020 \pm 0.002	0.06 \pm 0.01	0.40	0.3769	11.99	11.71	1.89
F16357 + 7658.....	271 \pm 25	0.51 \pm 0.11	268 \pm 16	260 \pm 20	400 \pm 100	19.6 (R)	2.30	0.044 \pm 0.004	0.09 \pm 0.01	0.85	0.2714	11.78	9.77	1.67

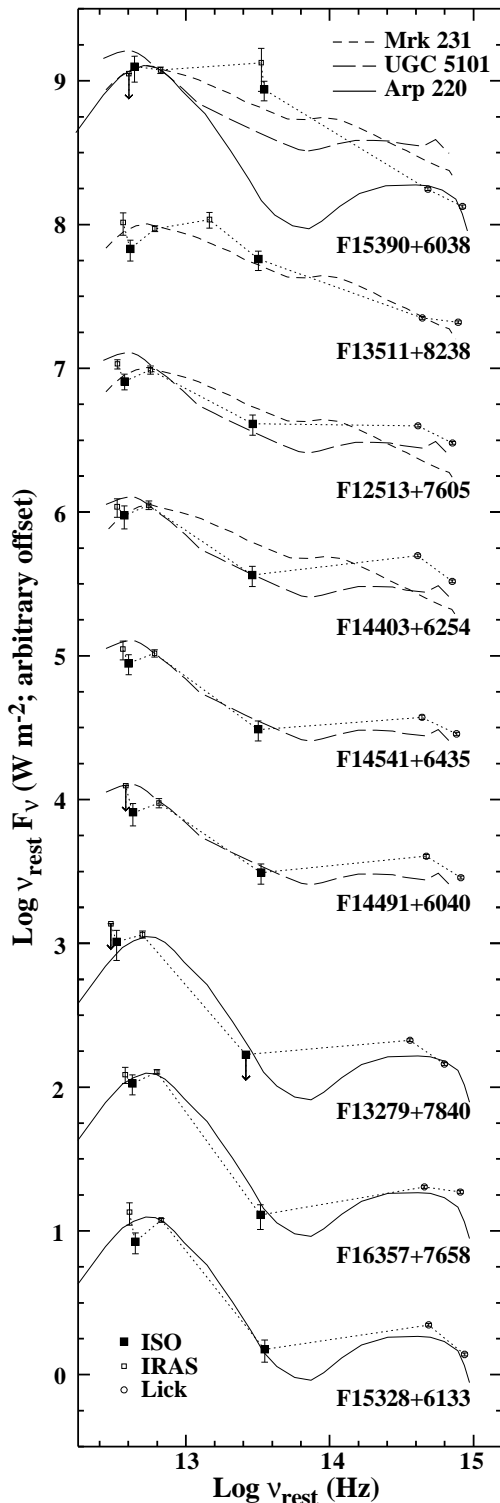


FIG. 4.—Rest frame FIR-optical spectral energy distributions for the nine IIFGS sources. Plotted from long to short wavelength are: (1) *IRAS* 100 μm SCANPI flux density, (2) 90 μm ISOPHOT flux density, (3) *IRAS* 60 μm flux density (also 25 and 12 μm *IRAS* data where detected), (4) 11.5 μm ISOCAM measure, and (5) Lick *I* ($\lambda 8275$) and *G* ($\lambda 4700$) band photometry. Error bars on the *ISO* fluxes include the estimated absolute calibration uncertainty of 30%. Spectra are ordered by steepness of the mid-infrared SED with arbitrary logarithmic offset. The IIFGS data points are connected by a dotted line. The SEDs of Arp 220 (pure starburst, solid line), UGC 5101 (intermediate AGN, long-dashed line), and Mrk 231 (infrared QSO, short-dashed line) are plotted for comparison. In each case we overplot the SED(s) that by visual inspection best match the IIFGS data. The spectrum of F15390 + 6038, a high excitation Seyfert 2 galaxy, is exceptional, with warm infrared color but steep IR-optical slope.

however, it is likely that two of the sample, F14541 + 6435 and F14403 + 6254, are disk systems. F14491 + 6040 is a particularly interesting source, showing a pair of galaxies that are clearly interacting, with a tidal tail (Fig. 2*b*). As shown in Figure 3, one of the pair shows H II excitation, and the other displays AGN excitation.

Figure 5 shows the infrared/optical photometric relationships compared with a local LIG sample, the BGS (Soifer et al. 1987), and 24 infrared-selected QSOs (R. M. Cutri 1998, private communication). Figure 5*a* shows that our selection for high far-infrared luminosity was successful since the nine IIFGS galaxies inhabit the upper end of the $L_{60\mu\text{m}}$ versus $L_{60\mu\text{m}}/L_{\text{blue}}$ relation for LIGs. Indeed, two of our objects lie right at the tip of the distribution (although samples of “hyperluminous” infrared galaxies [Cutri et al. 1994] have not been included on this plot). The IR QSOs separate well from the LIGs in this diagram, and the IIFGS galaxies resemble the LIGs more closely. However, Figure 5*b* shows that two of the IIFGS galaxies are unusually high in $L_{12\mu\text{m}}$ compared with the BGS sample, and one falls close to the region occupied by the IR QSOs. This object, F15390 + 6038, has the warmest mid-infrared SED of the sample and also displays the strongest evidence for AGN excitation. It peaks strongly in the mid-infrared, falling steeply into the optical, showing an unusually large value of $L_{12\mu\text{m}}/L_{\text{blue}}$. Thus it may be a new dust-obscured QSO. F13511 + 8238 also has a 12 μm luminosity, which is comparable to that of IR QSOs. It does not have a remarkably warm $S_{60\mu\text{m}}/S_{12\mu\text{m}}$ color, but it is the only object in our sample detected by *IRAS* at 25 μm (120 ± 30 mJy) with a very warm $S_{60\mu\text{m}}/S_{25\mu\text{m}}$ color. Thus it too may be a new dust-obscured QSO, although our spectroscopy has not identified any clear evidence for an active nucleus. Deep near-infrared spectroscopy of strong hydrogen lines or spectroscopy in polarized light of these two objects might reveal evidence for a dust-obscured or scattered broad-line region.

Three objects, F13279 + 7840, F15328 + 6133, and F16357 + 7658, show remarkably cool $S_{60\mu\text{m}}/S_{12\mu\text{m}}$ colors, apparently cooler than any of the BGS galaxies (Fig. 5*c*; F13279 + 7840 does not appear in Fig. 5*b* since it has no measured redshift). F13279 + 7840 and F16357 + 7658 exhibit evidence for AGN excitation, while F15328 + 6133 shows an H II optical spectrum. However, the *k*-corrections for F15328 + 6133 and F16357 + 7658 are substantial (see Fig. 4), and there are several possible biases that could cause a tendency toward large $S_{60\mu\text{m}}/S_{12\mu\text{m}}$ ratios in this sample. The first possible bias is due to the fact we can place a more sensitive limit on the $S_{60\mu\text{m}}/S_{12\mu\text{m}}$ color than possible for most *IRAS* samples, including the BGS, because the relative sensitivity of the *IRAS* 60 μm band is so much higher than the *IRAS* 12 μm band. Indeed, not all of the BGS sample was detected by *IRAS*, even when the data were co-added using the SCANPI processor, as shown by the upper limits in Figure 5*c*. Second, there may be a systematic tendency for the *IRAS* 60 μm flux densities of our sources to be overestimated, because they are close to the 60 μm sensitivity limit of the FSS: for sources just below the limit of a flux-limited sample, positive noise excursions bring a source into the sample while negative ones do not, so the average flux density of sources near the threshold is boosted (although a first-order correction for such effects was applied to the FSC; Moshir et al. 1992). Finally, we reiterate that the CAM photometry is still subject to some calibration uncertainty. We will address the influence of such biases in

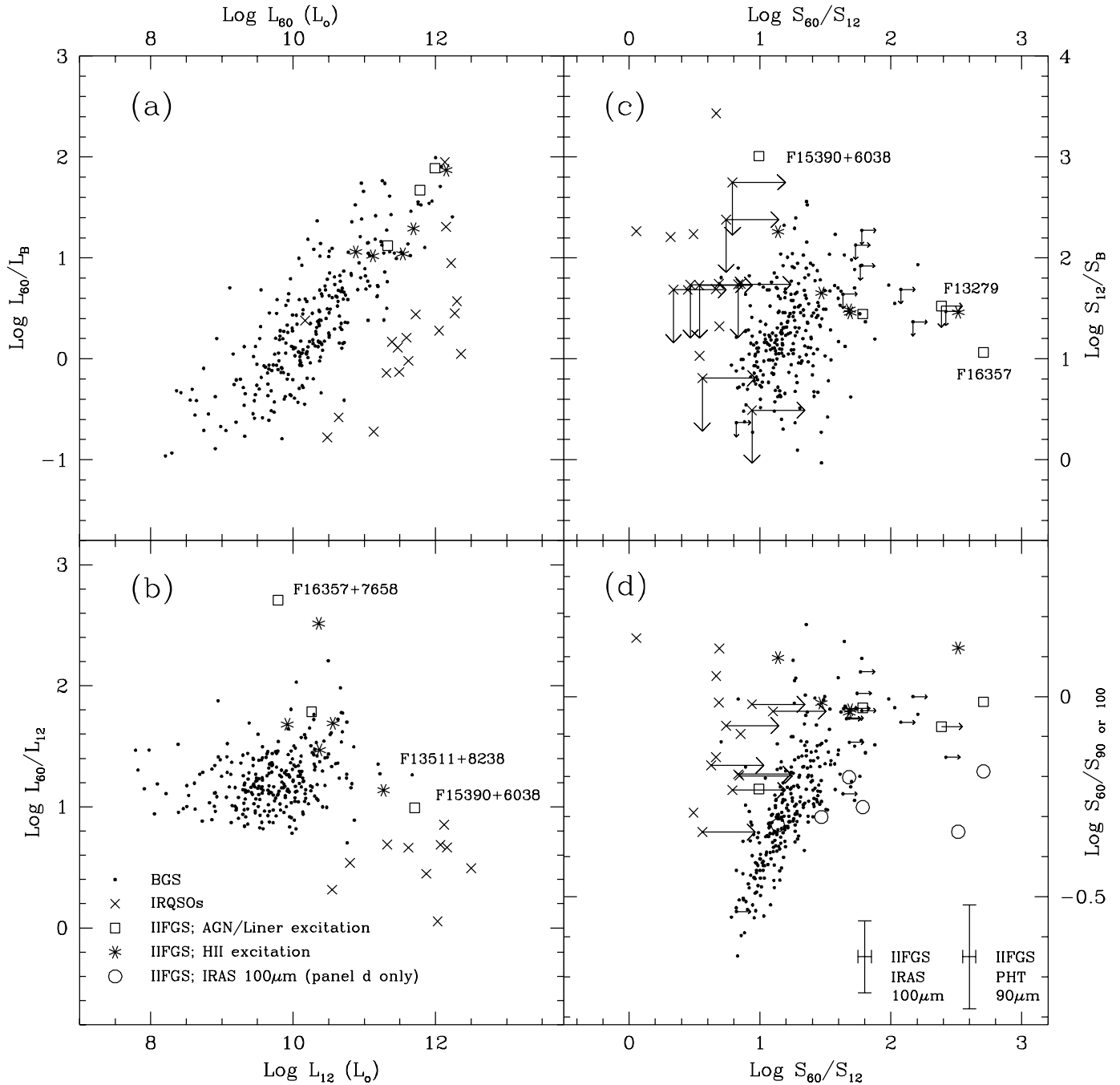


FIG. 5.—Distributions of flux-density ratios (colors) and luminosities for the nine IIFGS galaxies compared with the local universe BGS (Soifer et al. 1987) and infrared-selected QSOs (IR QSOs) (Cutri et al. 1994). (a) FIR/blue color–60 μm luminosity relationship. (b) 60 μm /12 μm color vs. 12 μm luminosity. (c) 12 μm /blue color ratio vs. 60 μm /12 μm color ratio. (d) 60 μm /100 μm color ratio vs. 60 μm /12 μm color ratio. The legend shown in panel b is the same for all panels, with representative *IRAS* and *ISO* error bars indicated in panel d. No *k*-corrections have been applied to the data as plotted. Individual IIFGS galaxies are indicated by name in panels b and c when they fall off the general BGS relationships, such as the IR QSO-like F15390+6038. In panel d IIFGS galaxies are plotted twice if they have both an *IRAS* 100 μm detection and a PHT 90 μm detection. Typical error bars for both ratios $S_{60 \mu\text{m}}/S_{90 \mu\text{m}}$ and $S_{60 \mu\text{m}}/S_{100 \mu\text{m}}$ are illustrated. Both the BGS and the IR QSOs include objects with only upper limits to the 12 μm *IRAS* flux density.

follow-up publications (Hurt et al. 1998; Lonsdale et al. 1998c) when the statistics of a large IIFGS sample are available and the calibration is more certain.

Figures 4 and 5d indicate that the longer wavelength photometry has a disappointingly high dispersion, but perhaps this was to be expected. As discussed previously, there is a systematic difference between the ISOPHOT 90 μm flux densities and the available *IRAS* 100 μm measures, with the *IRAS* 100 μm data being higher by about 0.25 dex.

However, both the PHT data and the *IRAS* 100 μm data have relatively low signal-to-noise ratios, and the ever-present concern about galactic cirrus contamination of the photometry lends further uncertainty to the point-source fluxes. Moreover, systematic sensitivity and calibration effects are still being assessed for the PHT C100 AOT. Therefore, a more detailed discussion of the longer wavelength photometry will be left to a later paper in this series.

4. SUMMARY AND FUTURE PROSPECTS

These first results from the IIFGS have shown that if this small sample of nine sources is representative of the whole, the IIFGS will be one of the largest and deepest samples of faint infrared-luminous galaxies available until the advent of WIRE (Hacking et al. 1996) and SIRTf. The redshift range for this sample is $0.1 \lesssim z \lesssim 0.4$, which is reasonably well predicted by use of the $L_{60\ \mu\text{m}}$ versus $L_{60\ \mu\text{m}}/L_{\text{blue}}$ relation for those objects for which the APM-measured blue magnitudes turned out to be close to the new *G*-band photometry. The ISOCAM detection rate is also impressively high, 80% for the sample of 418 IIFGS objects already processed, demonstrating that the *IRAS* galaxy selection techniques are highly robust against artifacts and cirrus-related sources. We can therefore expect that by the end of the *ISO* mission there will be on the order of 600 IIFGS galaxies with $0.1 \lesssim z \lesssim 1.0$, and $10^{10.5} \lesssim L_{60\ \mu\text{m}} \lesssim 10^{13}$, an excellent sample for study of the evolutionary history of infrared-luminous galaxies from ~ 5 Gyr ago to the present.

Our survey will also result in a serendipitous measurement of the $12\ \mu\text{m}$ galaxy number counts, since our field of view is quite large. We have already accumulated over $1.25\ \text{deg}^2$ of deep CAM imaging to an $11.5\ \mu\text{m}$ point-source completeness limit of approximately 1.0 mJy (corresponding to a $\sim 10\ \sigma$ detection sensitivity), comparable to other dedicated *ISO* deep cosmological surveys. Our first estimate of the $12\ \mu\text{m}$ log N -log S relationship will be presented by Lonsdale et al. (1998c).

The characteristics of the nine sources discussed here are

similar to those of the local *IRAS* BGS. They span a similar range of $60\text{--}12\ \mu\text{m}$ infrared spectral slope and infrared luminosity. There is also evidence that the flatter spectrum sources are more likely to house an active nucleus, and our highest redshift source, F15390 + 6038, has the flattest infrared spectral energy distribution and displays a Seyfert 2 type optical spectrum. It seems very similar to several of the luminous infrared-selected QSOs (R. M. Cutri 1998, private communication).

We wish to thank the staff of Lick Observatory for supporting the optical observations reported here, especially Rem Stone for measuring the filter curves and also K. H. Smith for tireless assistance with the observations. The ISOCAM data presented in this paper were reduced using components of CIA, a joint development by the ESA Astrophysics Division and the ISOCAM Consortium led by the ISOCAM PI, C. Cesarsky, Direction des Sciences de la Matière, CEA-Saclay, France. The ISOPHOT data were reduced using PIA, which is a joint development by the ESA Astrophysics Division and the ISOPHOT consortium. This project has benefited from the use of the NASA Extragalactic Database, supported at IPAC by NASA, and the STScI Digitized Sky Survey images of the Palomar Observatory Sky Survey. H. E. S. thanks IPAC for providing continuing support as a home away from home. IPAC/JPL is supported by NASA. Additional support of this project has been provided by NASA *ISO* grants to IPAC and to UCSD.

REFERENCES

- Baldwin, J. A., Phillips, M. M., & Terlevich, R. 1981, *PASP*, 93, 5
 Barvainis, R., Antonucci, R., Hurt, T., Coleman, P., & Reuter, H.-P. 1995, *ApJ*, 451, L9
 Cesarsky, C., et al. 1996, *A&A*, 315, L32
 Condon, J. J., Anderson, M., & Helou, G. 1991, *ApJ*, 376, 95
 Condon, J. J., et al. 1997, preprint
 Cutri, R. M., Huchra, J. P., Low, F. J., Brown, R. L., & Vanden Bout, P. A. 1994, *ApJ*, 424, L65
 Eisenhardt, P., Armus, L., Hogg, D., Soifer, B. T., Neugebauer, G., & Werner, M. 1996, *ApJ*, 461, 72
 Gabriel, C., Acosta-Pulido, J., Heinrichson, I., Morris, H., & Tai, M.-W. 1997, in *ASP Conf. Ser. 125, Astronomical Data Analysis Software and Systems VI*, ed. G. Hunt & H. Payne (San Francisco: ASP), 108
 Hacking, P. B. 1996, 388, 310
 Hurt, R., et al. 1998, in preparation
 Irwin, M. J., et al. 1994, *Gemini Newsl.* 37, Royal Astronomical Society
 ISOPHOT Instrument Dedicated Team. 1998, Internal Report
 Kennicutt, R. 1992, *ApJ*, 388, 310
 Kessler, M., et al. 1996, *A&A*, 315, L27
 Lemke, D., et al. 1996, *A&A*, 315, L64
 Lonsdale, C. J., Lonsdale, C. J., Diamond, P. D., & Smith, H. E. 1998a, *ApJ*, 494, L239
 Lonsdale, C. J., Lonsdale, C. J., & Smith, H. E. 1995, *BAAS*, 28, 1359
 Lonsdale, C. J., et al. 1997, in *IAU Symp. 179, New Horizons from Multi-wavelength Sky Surveys*, ed. B. McClean (Dordrecht: Kluwer)
 ———. 1998b, in preparation
 ———. 1998c, in preparation
 Moshir, M. M., et al. 1992, Explanatory Supplement to the *IRAS* Faint Source Survey, Version 2, JPL D-10015 (Pasadena: JPL)
 Sanders, D. B., & Mirabel, F. 1996, *ARA&A*, 34, 749
 Sanders, D. B., et al. 1988, *ApJ*, 325, 74
 Smith, H. E., et al. 1998a, in *The Young Universe*, ed. S. d'Odorico, A. Fontana & E. Giallongo (San Francisco: ASP), 220
 Smith, H. E., Lonsdale, C. J., & Lonsdale, C. J. 1998, *ApJ*, 492, 137
 Smith, H. E., Lonsdale, C. J., Lonsdale, C. J., & Diamond, P. 1998b, *ApJ*, 493, L17
 Soifer, B. T., et al. 1987, *ApJ*, 320, 238
 Sturm, E., et al. 1996, *A&A*, 315, L133
 Veilleux, S., Kim, D.-C., Sanders, D. B., Mazzarella, J., & Soifer, B. T. 1995, *ApJS*, 98, 171